Structural Requirements for Chemoselective Ammonolysis of Ethylene Glycol to Ethanolamine over Supported Cobalt Catalysts

Xianchi Lei, Guoding Gu, Yafei Hu, Haoshang Wang, Zhaoxia Zhang and Shuai Wang *

Collaborative Innovation Center of Chemistry for Energy Materials, State Key Laboratory for Physical Chemistry of Solid Surfaces, National Engineering Laboratory for Green Chemical Productions of Alcohols-Ethers-Esters, College of Chemistry and Chemical Engineering, Xiamen University, Xiamen 361005, China; leixianchi@stu.xmu.edu.cn (X.L.); guodinggu@stu.xmu.edu.cn (G.G.); yafeihu@stu.xmu.edu.cn (Y.H.); wanghaoshang@stu.xmu.edu.cn (H.W.); zzxyyy@xmu.edu.cn (Z.Z.)
* Correspondence: shuaiwang@xmu.edu.cn; Tel.: +86-0592-2182050

Abstract: Ethylene glycol is regarded as a promising C_2 platform molecule due to the fast development of its production from sustainable biomass. This study inquired the structural requirements of Co-based catalysts for the liquid-phase ammonolysis of ethylene glycol to value-added ethanolamine. We showed that the rate and selectivity of ethylene glycol ammonolysis on γ-Al_2O_3-supported Co catalysts were strongly affected by the metal particle size within the range of 2–10 nm, among which Co nanoparticles of ~4 nm exhibited both the highest ethanolamine selectivity and the highest ammonolysis rate based on the total Co content. Doping of a moderate amount of Ag further promoted the catalytic activity without affecting the selectivity. Combined kinetic and infrared spectroscopic assessments unveiled that the addition of Ag significantly destabilized the adsorbed NH_3 on the Co surface, which would otherwise be strongly bound to the active sites and inhibit the rate-determining dehydrogenation step of ethylene glycol.

Keywords: co-based catalyst; ethylene glycol; alcohol ammonolysis; ethanolamine; size effect of metal particles; Ag-doping

1. Introduction

Ethylene glycol is the simplest vicinal diol and has been applied as an essential raw chemical in various fields, such as solvent, antifreeze agent, surfactant, and plastics [1]. At present, the major industrial route of manufacturing ethylene glycol consists of hydrolysis of ethylene oxide, while the latter is obtained from partial oxidation of petroleum-derived ethylene. New routes are also explored to synthesize ethylene glycol from other carbon resources (e.g., syngas and renewable biomass feedstocks) [2,3]. Therefore, it is expected that such emerging non-petroleum routes will increase the availability and sustainability of the ethylene glycol supply and enable ethylene glycol to act as an alternative C_2 platform molecule to replace ethylene oxide, which is very reactive and difficult to handle and transport [4].

In this last context, the synthesis of ethanolamine is an illustrative example showing the potential replacement of ethylene oxide by ethylene glycol in the production of basic chemicals. Ethanolamine is widely used as an absorbent for CO_2 and SO_2 and building blocks for pharmaceuticals, agrochemicals, and detergents, having an annual demand of two million tons [5]. In the industry, ethanolamine is obtained, traditionally, by the ammonolysis of ethylene oxide carried out with excess of NH_3 [4]. An alternative, as an attractive industrial pathway, is the chemoselective ammonolysis of ethylene glycol when solely H_2O is the by-product (Scheme 1). However, the latter route generally requires a higher temperature (e.g., 453~523 K) to occur, under which condition ethanolamine can

readily convert to secondary amination products (e.g., piperazine, ethylenediamine, and diethanolamine) [6–9]. Consequently, developing novel catalysts for efficient formation of ethanolamine from ethylene glycol under mild conditions is highly desired.

(1) An industrial route using ethylene oxide as reactant

(2) An alternative route using ethylene glycol as reactant
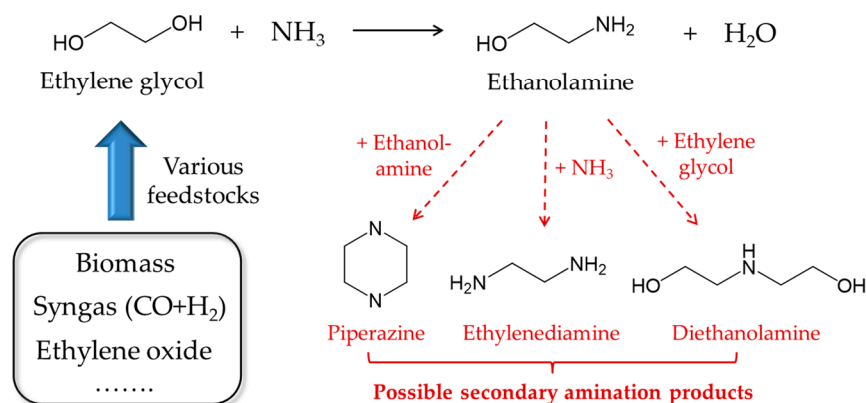
Scheme 1. Synthetic routes of ethanolamine formation from ethylene oxide and ethylene glycol.

　　Metal catalysts have been reported to be efficient in the ammonolysis of alcohols containing at least a primary or secondary hydroxyl group (e.g., aliphatic primary monohydric alcohols and dihydric primary alcohols) via a hydrogen-borrowing methodology [6,7,10–16]. This hydrogen-borrowing pathway generally consists of three elementary steps:

　　(1) Dehydrogenation of one of the hydroxyl group in the alcohol to form a C=O bond;

　　(2) Transformation of the C=O bond to a C=N bond through a nucleophilic attack by NH_3 and a subsequent dehydration.

　　(3) Hydrogenation of the C=N bond to give a primary amine using the hydrogen generated in the first step.

　　It is worth nothing that the primary amine product has higher nucleophilicity than NH_3 and is thus more reactive than the latter for the second step, which often leads to undesired formation of secondary amines [7]. Compared with the case of simple monohydric alcohols, both of the hydroxyl groups in ethylene glycol can be replaced by $-NH_2$ to form diethanolamine and the primary ethanolamine product can undergo a further cyclization to form piperazine (Scheme 1) [6]. These issues make the achievement of a high selectivity of ethanolamine from the ammonolysis of ethylene glycol quite challenging.

　　Although studies on the catalytic ammonolysis of ethylene glycol are still limited [7], various metal catalysts (such as Co [17–19], Ni [20,21], Cu [22], Ru [23,24], Pd [25], Pt [26]) have been applied for the hydrogen-borrowing amination of monohydric alcohols or the corresponding carbonyl compounds. Among them, Co, Ni, and Ru have drawn attention the most, because of their high activity and chemoselectivity for primary amines. It has also been reported that the size of the metal nanoparticles [7] and the doping with a second metal—Cu [27], Ag [28], Ru [29], Bi [30], Re [31], or Pt [32]—can significantly improve the catalyst performance, providing a basis for further optimizing the amination processes. For example, the liquid-phase ammonolysis of 1-octanol showed a higher chemoselectivity to the primary amine product on smaller supported Ru nanoparticles than those on larger ones, because the latter favored the self-coupling of primary amines [33]. The doping

of Ag with a moderate amount in γ-Al$_2$O$_3$-supported Co catalysts (i.e., Co/γ-Al$_2$O$_3$) exhibited a strong Co-Ag interaction, improving both the activity and chemoselectivity for the 1-octanol ammonolysis [34].

In this study, we attempt to systematically investigate the ammonolysis of ethylene glycol in liquid phase using Co/γ-Al$_2$O$_3$ as a model catalyst and inquire the structural requirements of Co-based catalysts for the chemoselective formation of ethanolamine from ethylene glycol. In doing so, the size of the Co nanoparticles was controlled by tuning the Co loading, and typical doping metals (i.e., Cu, Ag, and Ru) were introduced separately. The activity and selectivity of these catalysts for ethylene glycol ammonolysis were rigorously compared at similar conversions and correlated with the catalyst structure. For the optimized Co-Ag/γ-Al$_2$O$_3$ catalysts, kinetic and spectroscopic assessments were further conducted to unveil the nature of the Ag-doping effect at a molecular level.

2. Results and Discussion

2.1. Preparation and Caharacterization of Co/γ-Al$_2$O$_3$ Catalysts with Different Co Particle Sizes

Co/γ-Al$_2$O$_3$ catalysts with four different Co loadings of 2, 5, 10, and 15 wt% were first prepared by the incipient wetness impregnation and used in the ammonolysis of ethylene glycol. According to X-ray diffraction patterns (XRD, Figure S1 of the supporting information), the metallic Co nanoparticles in these catalysts were well dispersed when the Co loading was below 10 wt%, because only the 15 wt% Co/γ-Al$_2$O$_3$ sample exhibited apparent diffraction signals ascribable to the Co metal (e.g., $2\theta = 44.2°$, $51.5°$, and $75.9°$). These high Co dispersions imply a strong interaction between the Co$_2$O$_3$ species and the γ-Al$_2$O$_3$ support in the oxide precursors of the Co/γ-Al$_2$O$_3$ catalysts (i.e., Co$_2$O$_3$/γ-Al$_2$O$_3$), supported by the partially reducible nature of these γ-Al$_2$O$_3$-supported Co$_2$O$_3$ species below 1027 K (40.2–87.1% of the total Co amount, determined by the H$_2$-temperature-programmed reduction (H$_2$-TPR), Table 1 and Figure S2) [35,36]. The dispersions of the metallic Co atoms were further measured by the chemisorption of N$_2$O at 323 K, which is able to selectively oxidize the surface of the Co nanoparticles at mild conditions [37,38]. As shown in Table 1, the measured Co dispersion decreased gradually from 44.9% to 9.8% by increasing the Co loading from 2 wt% to 15 wt%, corresponding to an increase of the Co nanoparticle size from 2.1 to 9.7 nm. The average Co particle size of 5 wt% Co/γ-Al$_2$O$_3$ was also determined by transmission electron microscopy (TEM, 4.3 ± 0.2 nm, Figure S3), consistent with that obtained by the N$_2$O-chemisorption method (4.2 nm, Table 1). These results confirm that the Co particle size of the Co/γ-Al$_2$O$_3$ catalysts were successfully tuned by changing the Co loading.

Table 1. Mass loading, reducibility, dispersion, and particle size of Co for the Co/γ-Al$_2$O$_3$ catalysts used in this study.

Catalyst	Co Loading [a] (wt%)	Co Reducibility [b] (%)	Co Dispersion [c] (%)	Average Co Particle Size [c] (nm)
2 wt% Co/γ-Al$_2$O$_3$	1.7	40.2	44.9	2.1
5 wt% Co/γ-Al$_2$O$_3$	4.9	80.1	23.1	4.2 (4.3 ± 0.2 [d])
10 wt% Co/γ-Al$_2$O$_3$	9.8	85.3	14.9	6.4
15 wt% Co/γ-Al$_2$O$_3$	14.7	87.1	9.8	9.7

[a] determined by the inductively coupled plasma optical emission spectrometry. [b] estimated from the reducible content of Co below 1073 K in the H$_2$-TPR process of the oxide precursors of the Co/γ-Al$_2$O$_3$ catalysts (Figure S2a). [c] determined by the N$_2$O-chemisorptoion method (Figure S2b). [d] determined by TEM (Figure S3).

2.2. Effects of Co Particle Size for Co/γ-Al$_2$O$_3$ Catalysts in Ammonolysis of Ethylene Glycol

Ammonolysis of ethylene glycol on these Co/γ-Al$_2$O$_3$ catalysts were carried out at 453 K in tetrahydrofuran solvent with initial NH$_3$ and H$_2$ pressures of 0.6 and 3.0 MPa (0.13 mol/L ethylene glycol; ethylene glycol/NH$_3$/H$_2$ molar ratio = 1.0/8.5/42.5), respectively. For a rigorous comparison of the ammonolysis selectivity among these catalysts, the conversion of ethylene glycol for each catalyst was controlled at a similar level (~20%) by adjusting the catalyst amount loaded and the reaction time (2–4 h). On 2 wt% Co/γ-Al$_2$O$_3$

(2.1 nm Co), ethanolamine and glycolaldehyde were found as the main products with their carbon selectivity of 49.6% and 27.6%, respectively (Figure 1). According to the hydrogen-borrowing mechanism, glycolaldehyde, formed from dehydrogenation of ethylene glycol on the Co sites, served as an active intermediate for the ammonolysis of ethylene glycol ethanolamine (Scheme 2). It is worth noting that glycolaldehyde may exist in the dimeric form instead of the monomeric form in the reaction solution, because the former state is thermodynamically more stable. Minor products mainly included those formed from secondary amination of ethanolamine (ethylenediamine, piperazine) and dehydration of ethylene glycol (ethylene oxide, ethanol, diethylene glycol).
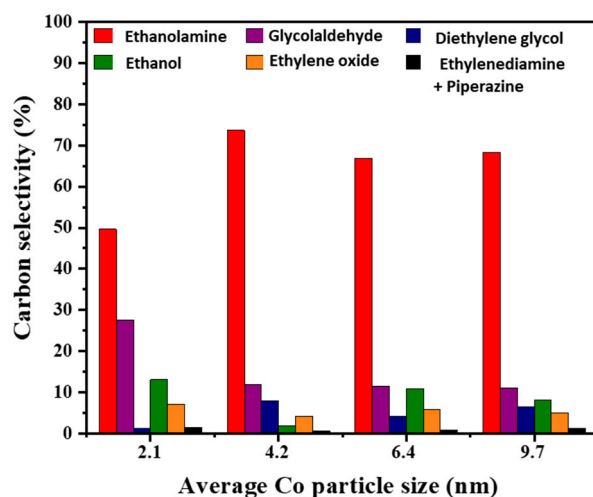
Figure 1. Effects of Co particle size on the carbon selectivity of ammonolysis of ethylene glycol on Co/γ-Al$_2$O$_3$ catalysts (453 K, 0.13 mol/L ethylene glycol in tetrahydrofuran solution, 0.6 MPa NH$_3$, 3.0 MPa H$_2$, controlled at ~20% conversion).
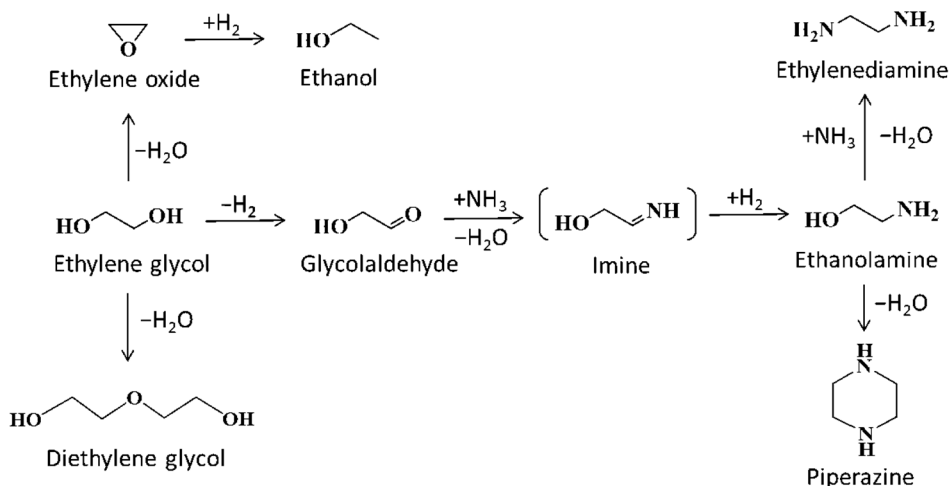
Scheme 2. Proposed reaction pathways for ethylene glycol conversion on Co/γ-Al$_2$O$_3$ in the presence of NH$_3$ and H$_2$ based on the products detected.

As the average Co particle size increased from 2.1 nm (2 wt% Co/γ-Al$_2$O$_3$) to 4.2 nm (5 wt% Co/γ-Al$_2$O$_3$), the carbon selectivity of ethanolamine significantly increased from 49.6% to 73.6%, concomitant with a decrease of the carbon selectivity of glycolaldehyde from 27.6% to 11.8% (Figure 1). This indicates that larger Co nanoparticles favor the C-N coupling between glycolaldehyde and NH$_3$. A further increase of the average Co particle size from 4.2 to 9.7 nm (i.e., 15 wt% Co/γ-Al$_2$O$_3$) led to the selectivity of ethanolamine decreased slightly from 73.6% to 69.3%, mainly because of an increase of the ethanol

selectivity from 1.9% to 8.1% (Figure 1). These data show that the selectivity of ethylene glycol ammonolysis was sensitive to the size of the Co nanoparticles and those with an average size of ~4.2 nm appear to be most selective to ethanolamine.

The effect of Co particle size on the ammonolysis activity of the Co/γ-Al$_2$O$_3$ catalysts was also apparent. As shown in Figure 2a, the rate of ethylene glycol conversion normalized by the exposed metallic Co atoms (i.e., the turnover frequency, TOF) gradually increased from 5.5 to 14.5 mol (mol$_{Co\text{-surface}}\cdot$h)$^{-1}$ when the average Co particle size was changed from 2.1 to 6.4 nm, but then declined to 11.1 mol (mol$_{Co\text{-surface}}\cdot$h)$^{-1}$ as the Co particle size further increased to 9.7 nm. Accordingly, the Co nanoparticles of around 6.4 nm (i.e., 10 wt% Co/γ-Al$_2$O$_3$) possessed the highest intrinsic activity for ethylene glycol conversion among the examined catalysts. As elucidated in Section 2.5, the rate-determining step of ethylene glycol ammonolysis on Co/γ-Al$_2$O$_3$ was the dehydrogenation of ethylene glycol to glycolaldehyde, and the observed effect of the Co particle size reflected, in fact, the corresponding difference of the dehydrogenation ability of the Co catalysts. When the rates of the ethylene glycol reaction were compared based on the total Co amount of the catalyst in order to assess the utilization efficiency of the Co metal, a similar trend of the rate change with the Co particle size was obtained (Figure 2b), while the maximum shifted to 5 wt% Co/γ-Al$_2$O$_3$ (4.2 nm Co) as a result of its higher Co dispersion than that for 10 wt% Co/γ-Al$_2$O$_3$.
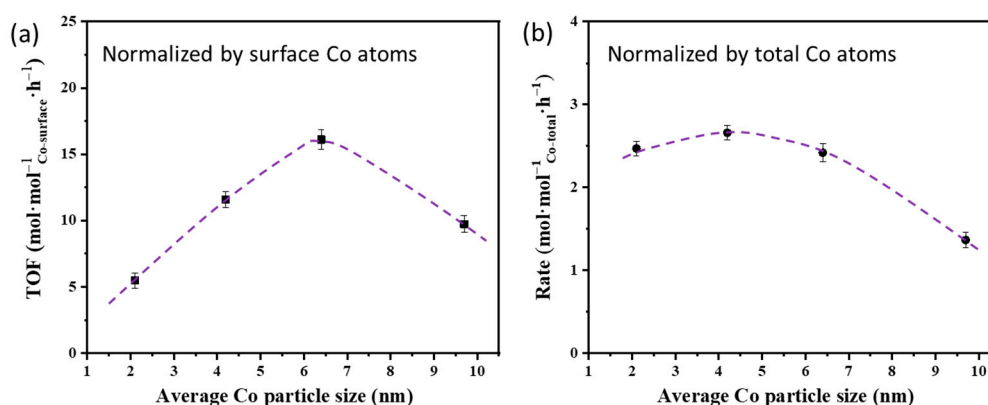
Figure 2. Effects of Co particle size on the rate of ethylene glycol conversion over Co/γ-Al$_2$O$_3$ catalysts normalized by (**a**) the surface Co atoms and (**b**) the total Co atoms (453 K, 0.13 mol/L ethylene glycol in tetrahydrofuran solution, 0.6 MPa NH$_3$, 3.0 MPa H$_2$, controlled at ~20% conversion). Dashed lines indicate trends.

Taken together, the above results clearly show that ammonolysis of ethylene glycol on the Co/γ-Al$_2$O$_3$ catalysts was a typical structure-sensitive reaction, as observed widely for ammonolysis of monohydric alcohols [7]. Considering 5 wt% Co/γ-Al$_2$O$_3$ (4.2 nm Co) exhibited the highest overall catalytic activity for ethylene glycol conversion and also the highest chemoselectivity of ethanolamine, this catalyst was used next as a reference for investigating the effects of metal-doping on the catalytic performance of the Co/γ-Al$_2$O$_3$ catalysts.

2.3. Preparation and Caharacterization of Co/γ-Al$_2$O$_3$ Catalysts Doped by a Second Metal

Cu, Ag, and Ru metals were chosen here as a second component to modify the 5 wt% Co/γ-Al$_2$O$_3$ catalyst. These bimetallic catalysts were prepared via a co-impregnation method with the molar ratio of Co/M (M = Cu, Ag, Ru) fixed at 98.5/1.5 (denoted as Co$_{98.5}$M$_{1.5}$/γ-Al$_2$O$_3$ henceforth). Cu(NO$_3$)$_2$, AgNO$_3$, and RuCl$_3$ were chosen here as the dopant precursor, which were converted to the corresponding oxide and metallic states sequentially during the catalyst preparation (details in Section 3.1). As shown in Figure 3a, the introduction of Cu, Ag, or Ru metals into 5 wt% Co/γ-Al$_2$O$_3$ did not bring any observable change to the XRD pattern of the catalysts. In other words, no diffraction signals belonging to Co or the second metal appeared, indicating both of the metals

dispersed well on the γ-Al_2O_3 support. The energy-dispersive X-ray spectroscopy (EDS) mapping of these bimetallic catalysts confirmed the homogeneous distribution of the two metal elements ($Co_{98.5}Ag_{1.5}/\gamma$-Al_2O_3 as an example shown in Figure 3b–d). Further TEM characterization revealed that the addition of the second metal slightly decreased the size of the Co nanoparticles (e.g., from 4.3 ± 0.2 to 4.0 ± 0.3 nm in the case of $Co_{98.5}Ag_{1.5}/\gamma$-Al_2O_3, Figures S3 and S4).
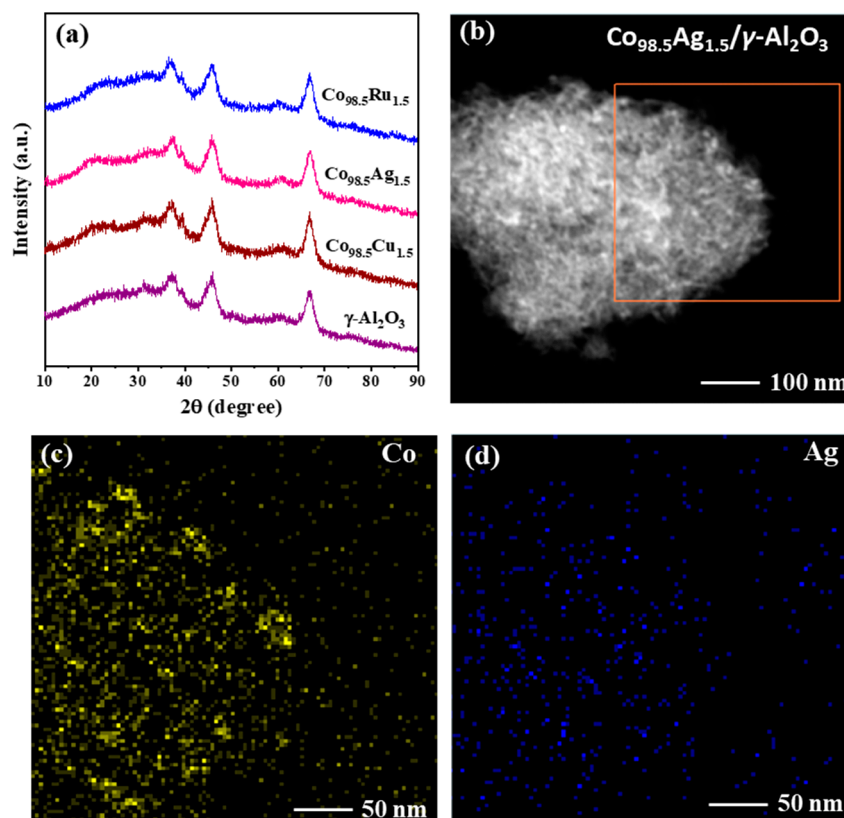
Figure 3. (**a**) Powder X-ray diffraction patterns for $Co_{98.5}M_{1.5}/\gamma$-Al_2O_3 (M = Cu, Ag, Ru; 5 wt% Co) samples with the γ-Al_2O_3 support as reference; (**b**) scanning transmission electron microscopy images for $Co_{98.5}Ag_{1.5}/\gamma$-Al_2O_3 with inserted EDS mapping of (**c**) Co and (**d**) Ag elements for the selected region.

The interaction between Co and the second metal in the $Co_{98.5}M_{1.5}/\gamma$-Al_2O_3 catalysts was assessed by the H_2-TPR process of their oxide precursors (i.e., $Co_{98.5}M_{1.5}O_x/\gamma$-$Al_2O_3$), which were obtained after the thermal treatment (in air, 673 K, 4 h) involved in the catalyst preparation process (details in Section 3.1). The overlapped multiple reduction peaks within the wide temperature range of 473-1073 K for the monometallic Co/γ-Al_2O_3 sample reflect the stepwise nature of the Co_2O_3 specie during their reduction by H_2 (Figure 4a). When metallic Cu was introduced into the Co/γ-Al_2O_3 catalyst, the shape of the H_2-TPR profile was only slightly changed with the reduction peaks shifted to low temperature by ~6 K, and the reduction degrees of the Co_2O_3 specie for Co/γ-Al_2O_3 and $Co_{98.5}Cu_{1.5}/\gamma$-Al_2O_3 were similar (80% vs. 77%, Figure 4b), indicative of a weak interaction between Co and Cu in $Co_{98.5}Cu_{1.5}/\gamma$-Al_2O_3. In contrast, the addition of Ag rendered the reduction of the Co_2O_3 specie much easier, exhibiting one broad reduction peak centered at 616 K. The reduction degree of $Co_{98.5}Ag_{1.5}/\gamma$-Al_2O_3 was also higher than that for Co/γ-Al_2O_3 (86% vs. 80%, Figure 4b). These changes revealed that the presence of Ag promoted the reduction of the Co_2O_3 specie, suggesting a close contact between Ag and Co in $Co_{98.5}Ag_{1.5}/\gamma$-Al_2O_3. Similar with the case of Ag doping, $Co_{98.5}Ru_{1.5}/\gamma$-Al_2O_3 showed a main reduction peak centered at 635 K, while it also had a minor reduction peak appearing at 478 K that was

likely relevant to the reduction of RuO_x or highly dispersed Co_2O_3 species. The reduction degree of $Co_{98.5}Ru_{1.5}/\gamma$-Al_2O_3 reached 1.0 (Figure 4b), reflecting a strong promoting effect of Ru doping on the reduction of the Co_2O_3 specie. The above distinct changes of the H_2-TPR process brough forth by the addition of Cu, Ag, and Ru metals suggested the catalytic performance of $Co_{98.5}M_{1.5}/\gamma$-Al_2O_3 would be influenced by these doped metals to different extents.
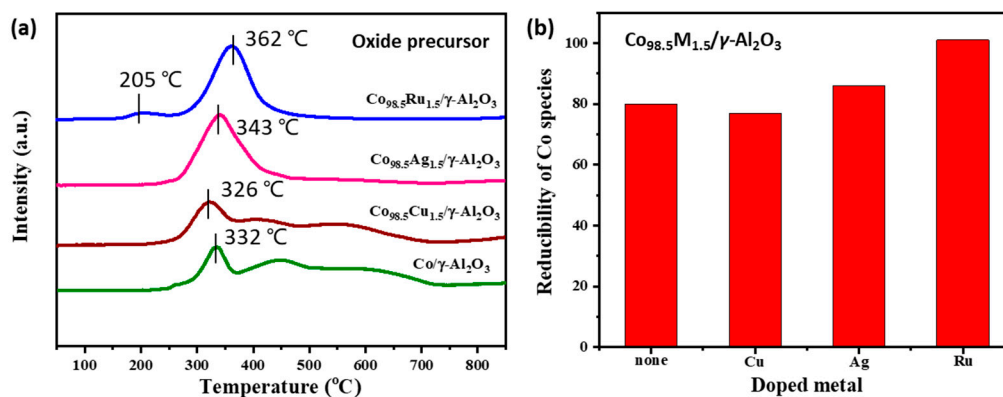
Figure 4. (**a**) H_2 temperature-programmed reduction profiles for the oxide precursors of $Co_{98.5}M_{1.5}/\gamma$-Al_2O_3 (M = Cu, Ag, Ru; 5 wt% Co) samples (i.e., $Co_{98.5}M_{1.5}O_x/\gamma$-$Al_2O_3$) and (**b**) the effects of the doped metal on the reduction degree of the Co specie in these reduction processes.

2.4. Effects of Doping a Second Metal for Co/γ-Al₂O₃ Catalysts in Ammonolysis of Ethylene Glycoy

As shown in Figure 5, the addition of Cu, Ag, or Ru metal improved the catalytic activity of Co/γ-Al_2O_3 in ammonolysis of ethylene glycol (453 K, 0.067 mol L^{-1} ethylene glycol, 0.6 MPa NH_3, 3.0 MPa H_2), and the reaction rates based on the total Co amount increased with an order of Cu, Ag, and Ru. However, it is noticeable that only $Co_{98.5}Ag_{1.5}/\gamma$-Al_2O_3 maintained a high selectivity of ethanolamine (72.7%) similar to that of the monometallic Co/γ-Al_2O_3 catalyst (72.2%) at ~20% conversion of ethylene glycol. The selectivity of ethanolamine decreased significantly in the presence of Cu (16.9%) or Ru (50.5%), in concomitance with an obvious increase of the selectivity of ethanol (Figure S5), which was ascribable to the high activity of Cu and Ru for hydrogenolysis of C-O bonds in polyols [39]. Therefore, compared with Cu and Ru, the doped Ag exhibited a superior ability to promote the selective ammonolysis of ethylene glycol to ethanolamine on Co/γ-Al_2O_3.

In order to optimize the promoting effect of Ag doping, Co-Ag/γ-Al_2O_3 catalysts with the Ag/(Co+Ag) atomic ratio ranged from 0 to 10% were prepared. On one hand, the rate of ethylene glycol conversion based on the total Co amount increased from 1.43 to 2.53 mol $(mol_{Co\text{-}total}\cdot h)^{-1}$ with increasing the Ag content from 0 to 5%, but then declined to 1.50 mol $(mol_{Co\text{-}total}\cdot h)^{-1}$ as the Ag content further increased to 10% (453 K, 0.067 mol L^{-1} ethylene glycol, 0.6 MPa NH_3, 3.0 MPa H_2; Figure 6). On the other hand, the selectivity of ethanolamine on the Co-Ag/γ-Al_2O_3 catalysts was nearly insensitive to the Ag content and kept around 73% at ~20% conversion of ethylene glycol for these bimetallic Co-Ag catalysts. Extra experiments confirmed that 5 wt% Ag/γ-Al_2O_3 was almost inert for catalyzing ammonolysis of ethylene glycol at the same reaction condition (Figure S6). Moreover, X-ray photoelectron spectroscopy (XPS) characterization showed that the Ag element was enriched on the Co-Ag/γ-Al_2O_3 catalysts. For instance, the measured surface Ag/(Co+Ag) atomic ratios for $Co_{98.5}Ag_{1.5}/\gamma$-Al_2O_3 and $Co_{95}Ag_5/\gamma$-Al_2O_3 were 3.2% and 6.4%, respectively (Figure S7), in line with the lower sublimation heat of Ag than that for Co (287 vs. 426 kJ mol^{-1}). These data implied that the doped Ag metal promoted the activity of the Co/γ-Al_2O_3 catalysts via surface modification, but too high Ag concentrations would inhibit the ammonolysis of ethylene glycol because of the dilution of the active Co sites.
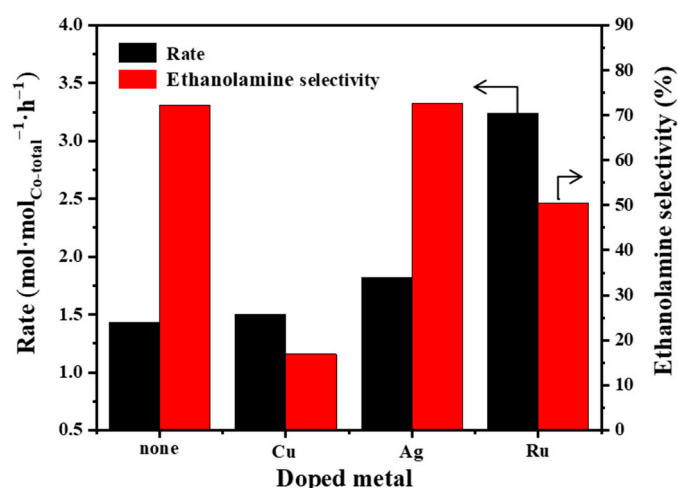
Figure 5. Effects of metal-doping on the rate and selectivity of the $Co_{98.5}M_{1.5}/\gamma$-Al_2O_3 (M = Cu, Ag, and Ru; 5 wt% Co) catalysts in ammonolysis of ethylene glycol (453 K, 0.6 MPa NH_3, 3.0 MPa H_2, 0.067 mol/L ethylene glycol in tetrahydrofuran solution, controlled at ~20% conversion).
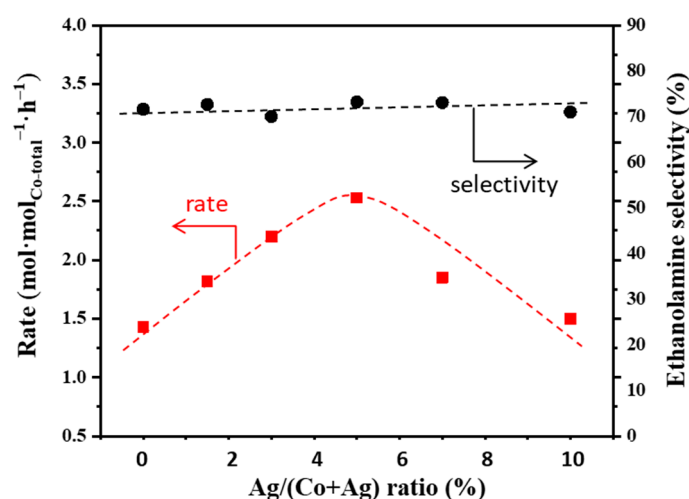
Figure 6. Effects of Ag content on the rate and selectivity of the Co-Ag/γ-Al_2O_3 (Co 5 wt%) catalysts in ammonolysis of ethylene glycol (453 K, 0.6 MPa NH_3, 3.0 MPa H_2, 0.067 mol/L ethylene glycol in tetrahydrofuran solution, controlled at ~20% conversion). Dashed lines indicate trends.

2.5. Kinetic Insights into the Ag-Doping Effects on Co/γ-Al_2O_3 Catalysts

In an attempt to unveil the nature of the Ag-doping effects, kinetic assessments were carried out for the Co/γ-Al_2O_3 and $Co_{98.5}Ag_{1.5}/\gamma$-Al_2O_3 samples with their Co loadings fixed at 5 wt%. These control experiments were done by varying the concentrations of ethylene glycol, NH_3, and H_2 individually at 453 K (Figure 7a–c), and the conversions of ethylene glycol were kept at ~20% as described in Section 2.2. The stirring speed of the autoclave reactor was set at 800 rpm, which was confirmed to be high enough to avoid any significant mass diffusion limitation at the examined reaction condition. It was observed that the ammonolysis of ethylene glycol to ethanolamine acted as the predominant reaction pathway in these control experiments, as reflected from the high chemoselectivities of ethanolamine (>70%) in most of the cases (Figures S8–S10). It is also worth noting that the product distribution of ethylene glycol conversion on the Co-based catalysts were not influenced strongly by the concentrations of ethylene glycol, NH_3, and H_2 (Figures S8–S10). Therefore, the following discussion was only focused on the effects of these reactants on the rates of ethylene glycol ammonolysis.

Table 2. Regressed kinetic parameters for ammonolysis of ethylene glycol on $Co/\gamma\text{-}Al_2O_3$ and $Co_{98.5}Ag_{1.5}/\gamma\text{-}Al_2O_3$ catalysts (Co 5 wt%) at 453 K.

Catalyst	k_{2+} (h^{-1})	K_1 (L·mol^{-1})	K_6 (MPa^{-1})	$k_2 + K_1$ (L·mol^{-1}·h^{-1})
$Co/\gamma\text{-}Al_2O_3$	1.4	4.9	8.0	6.9
$Co_{98.5}Ag_{1.5}/\gamma\text{-}Al_2O_3$	1.6	3.2	3.3	5.2
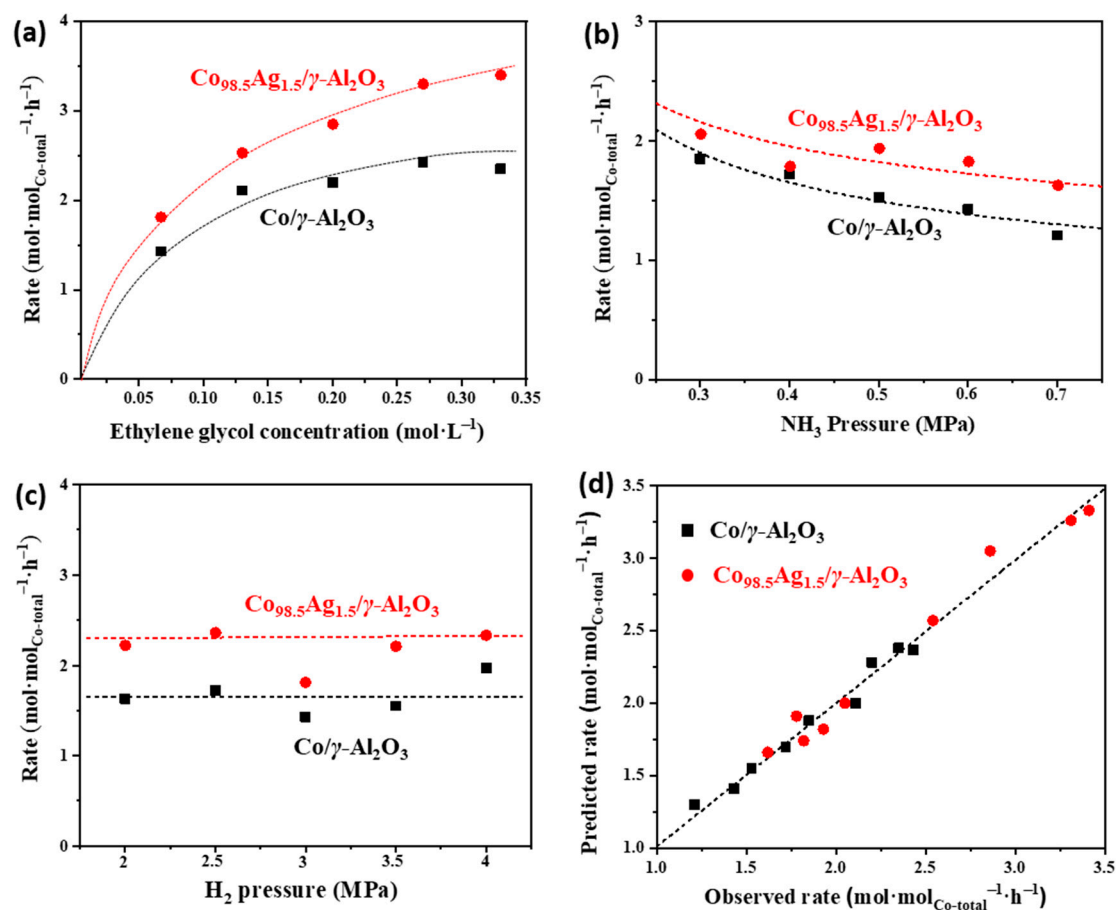
Figure 7. Rates of ethylene glycol concentration on the $Co/\gamma\text{-}Al_2O_3$ and $Co_{98.5}Ag_{1.5}/\gamma\text{-}Al_2O_3$ catalysts (Co 5 wt%) as functions of (**a**) ethylene glycol concentration, (**b**) NH_3 pressure, and (**c**) H_2 pressure (453 K, ~20% ethylene glycol conversion obtained by varying the catalyst amount or reaction time (2–4 h); (**a**) 0.6 MPa NH_3, 3.0 MPa H_2; (**b**) 3.0 MPa H_2, 0.067 mol/L ethylene glycol in tetrahydrofuran solution; (**c**) 0.6 MPa NH_3, 0.067 mol/L ethylene glycol in tetrahydrofuran solution). Dashed curves represent regressed fits to the functional form of Equation (1). (**d**) A parity plot for the measured and predicted rates of ethylene glycol amination (Equation (1)) on the $Co/\gamma\text{-}Al_2O_3$ and $Co_{98.5}Ag_{1.5}/\gamma\text{-}Al_2O_3$ catalysts with the regression-fitted parameters shown in Table 2.

As the concentration of ethylene glycol, NH_3, or H_2 was changed, the rate of ethylene glycol conversion on $Co_{98.5}Ag_{1.5}/\gamma\text{-}Al_2O_3$ varied in a manner similar to that on $Co/\gamma\text{-}Al_2O_3$ (Figure 7), albeit the bimetallic catalyst showed higher rates. These similar trends of rate change were indicative for the reaction mechanism of ethylene glycol conversions on the Co-based catalysts being unaltered by the doping of Ag. Specifically, the rates for the Co-based catalysts increased gradually as the concentration of ethylene glycol changed from 0.067 to 0.33 mol L^{-1} (Figure 7a), while the rate dependence on the concentration became weaker at higher concentrations, which is likely ascribable to an increase of the coverage of adsorbed ethylene glycol on the active Co sites. In contrast, the rates of ethylene glycol conversion were inhibited by increasing the partial pressure of NH_3 within the range of 0.3–0.7 MPa

(Figure 7b), indicative of strong adsorption of NH_3 on the active Co sites under the reaction condition and thus a negative reaction order with respect to NH_3. Different from the effects of ethylene glycol and NH_3, the rates of ethylene glycol conversion were nearly insensitive to the partial pressure of H_2 within the range of 2.0–4.0 MPa (Figure 7c), reflecting a typical zero-order kinetics as also observed for amination of alcohols on Cu-based catalysts [40].

As illustrated in Section 2.2 (Scheme 2), the ammonolysis of ethylene glycol mainly consists of three steps, including (1) dehydrogenation of ethylene glycol to glycolaldehyde, (2) condensation between glycolaldehyde and NH_3 to imine, (3) hydrogenation of imine to ethanolamine. The measured rate dependance on the pressures of NH_3 and H_2 excluded the kinetic relevance of the second and third steps to the conversion of ethylene glycol, otherwise a positive reaction order with respect to NH_3 or H_2 would be observed. Consequently, dehydrogenation of ethylene glycol to glycolaldehyde appeared to be rate-determining, consistent with previous studies on the ammonolysis of ethylene glycol [41] and other alcohols [7,10,14,42–44]. In particular, the dehydrogenation of ethylene glycol on the metal surface involves an initial O-H cleavage to form an alkoxide-type intermediate (Step 2, Scheme 3) and a subsequent abstraction of the α-H atom in this intermediate to form glycolaldehyde (Step 3, Scheme 3). Kinetic analysis was applied next to discern the kinetic relevance of these two steps.

Scheme 3. Proposed sequence of elementary steps for the kinetically-relevant dehydrogenation of ethylene glycol on metal surface. Reaction numbers used throughout the text are in parentheses (e.g., (1)); k_{i+}, k_{i-}, and K_i ($i = 1-6$) represent the kinetic constant for the forward step, the kinetic constant for the backward step, and the equilibrium constant for reaction i, respectively. Quasi-equilibrated steps are noted by a circle over double arrows.

If the O-H cleavage step was rate-determining and irreversible on the Co sites (Step 2 in Scheme 3), taken together with the assumptions for the quasi-equilibrated nature of the adsorption/desorption processes on the catalyst surface and the adsorbed ethylene glycol and NH_3 as the predominant surface species, the rate equation for ethylene glycol conversion (r_{EG}) on the Co-based catalysts is given by:

$$r_{EG} = \frac{k_{2+}K_1[EG]}{(1 + K_1[EG] + K_6[NH_3])^2} \tag{1}$$

Here, [EG] and [NH_3] are the concentrations of ethylene glycol and NH_3, respectively, and K_1 and K_6 are the corresponding adsorption constants for these two reactants. The k_{2+} term is the forward kinetic constant for the O-H cleavage step, representing the intrinsic

ability of the active Co sites to cleave the O-H bond. As shown in Figure 7d, an excellent fitness of Equation (1) with the rates of ethylene glycol ammonolysis was found for both of the Co/γ-Al$_2$O$_3$ and Co$_{98.5}$Ag$_{1.5}$/γ-Al$_2$O$_3$ catalysts, supporting the hypothesis that the initial activation of O-H bond in ethylene glycol is the rate-determining step.

In constant, if the α-H abstraction of the alkoxide-type intermediate (Step 3 in Scheme 3) was the irreversible rate-determining step instead, r_{EG} is converted to the form as

$$r_{EG} = \frac{k_{3+}K_1K_2K_5^{-1}[EG][H_2]^{-1/2}}{(1 + K_1[EG] + K_6[NH_3])^2} \tag{2}$$

in which [H$_2$] and K_5 are the concentration and adsorption constant for H$_2$, respectively, k_{3+} is the forward kinetic constant for the α-H abstraction step, and K_2 is the equilibrium constant for the O-H cleavage step (equal to k_{2+}/k_{2-} with k_{2-} as the backward kinetic constant for this step). Equation (2) indicates that r_{EG} is inhibited by H$_2$ because of the $-1/2$ order of H$_2$ appeared in the numerator, inconsistent with the measured zero-order rate dependance (Figure 7c). As expected, a poor fitness of Equation (2) with the rate data of ethylene glycol ammonolysis was obtained (Figure S11). Therefore, the kinetic relevance of the α-H abstraction step was ruled out.

Table 2 compared the regression-fitted parameters of Equation (1) for the Co/γ-Al$_2$O$_3$ and Co$_{98.5}$Ag$_{1.5}$/γ-Al$_2$O$_3$ catalysts. It was shown that the doping of 1.5% Ag led to a slight increase of k_{2+} from 1.4 to 1.6 h^{-1}, while the values of K_1 and K_6 declined from 4.9 to 3.2 L mol^{-1} and from 8.0 to 3.3 MPa^{-1}, respectively. As a consequence, the $k_{2+}K_1$ term in the numerator of Equation (1) was slightly higher on the Co/γ-Al$_2$O$_3$ catalyst than that for Co$_{98.5}$Ag$_{1.5}$/γ-Al$_2$O$_3$ (6.9 vs. 5.2 L (mol·h)$^{-1}$), suggesting the presence of Ag, in fact, increased the apparent activation barrier of the O-H cleavage on the Co surface and made the Co catalyst intrinsically less active. On the other hand, the decrease of the values for K_1 and K_6 brought forth by the Ag-doping indicated that the Co active sites on Co$_{98.5}$Ag$_{1.5}$/γ-Al$_2$O$_3$ were less covered by ethylene glycol and NH$_3$ compared with the case of Co/γ-Al$_2$O$_3$. Under the reaction condition typically used in this study (453 K, 0.067 mol L^{-1} ethylene glycol, 0.6 MPa NH$_3$, 3.0 MPa H$_2$), the coverages of ethylene glycol and NH$_3$, estimated by the K_1 and K_6 terms, were 5% and 78% for Co/γ-Al$_2$O$_3$, respectively, while these coverages for Co$_{98.5}$Ag$_{1.5}$/γ-Al$_2$O$_3$ were changed to 7% and 62%, respectively. It can be seen that the adsorbed NH$_3$ was the predominate surface species during ammonolysis of ethylene glycol on both of the catalysts. More importantly, the addition of Ag into the Co surface significantly weakened the adsorption of NH$_3$ and made the percentage of the unoccupied active Co sites nearly double (16% vs. 31%), which probably accounted for the promoting effect of Ag-doping on the rate of ethylene glycol ammonolysis.

According to the above kinetic analysis, the Ag dopant mainly acted as an inhibitor for the adsorptions of NH$_3$ and ethylene glycol on the Co metal surface (based on the changes of K_6 and K_1, respectively, Table 2) and did not significantly affect the intrinsic activity of the Co sites (based on the change of k_{2+}, Table 2). This conclusion is consistent with the negligible activity of monometallic Ag/γ-Al$_2$O$_3$ catalysts in ammonolysis of ethylene glycol at the reaction condition of this study (Figure S6). A recent theoretical study also showed that the Ag dopant had a weak effect on the intrinsic activity of Co catalysts for ammonolysis of methanol [29]. However, it is worth emphasizing that the above kinetic treatment was based on an ideal assumption that the Co$_{98.5}$Ag$_{1.5}$/γ-Al$_2$O$_3$ catalyst possessed uniform active sites. The Ag dopant may lead to the formation of Co-Ag surface site pairs or even single-atom alloys that are highly active for dehydrogenation of ethylene glycol, considering that Ag-based catalysts have been widely used for alcohol dehydrogenation [45,46]. This latter possibility cannot be excluded because of the lack of atomic-level structural characterization at the current stage of our study.

2.6. Spectroscopic Evidence for the Ag-Doping Effect on the Stability of Adsorbed NH$_3$ Species

Diffuse reflectance infrared Fourier transform spectroscopy (DRIFTS) was further applied to validate the effect of Ag-doping on the stability of adsorbed NH$_3$ species. The pre-adsorption of NH$_3$ on Co/γ-Al$_2$O$_3$, Co$_{98.5}$Ag$_{1.5}$/γ-Al$_2$O$_3$ and the γ-Al$_2$O$_3$ support was conducted at the real condition of catalytic ammonolysis (453 K, 0.067 mol L^{-1} ethylene glycol in tetrahydrofuran, 0.6 MPa NH$_3$, 3.0 MPa H$_2$), and the resultant samples were treated in vacuum to remove the physically adsorbed NH$_3$, ethylene glycol, and tetrahydrofuran before acquiring infrared spectra. Using the spectra collected at ambient temperature as the background, three reverse IR bands appeared at around 1651, 1486, and 1432 cm^{-1} within the range of 1200–1800 cm^{-1} for both of Co/γ-Al$_2$O$_3$ and Co$_{98.5}$Ag$_{1.5}$/γ-Al$_2$O$_3$ at 343 K (Figure 8a), which reflected the desorption of chemically bound species from the catalyst surface. In contrast, the γ-Al$_2$O$_3$ support merely exhibited the IR band at ~1651 cm^{-1}, assignable to the NH$_4^+$ ions formed from the adsorption of NH$_3$ on the Brønsted acid sites of γ-Al$_2$O$_3$ [47,48]. Therefore, the two bands at 1486 and 1432 cm^{-1} appeared to be derived from those adsorbed on the Co surface. Specifically, the band at 1486 cm^{-1} was attributable to the C-C stretching/C-H bending vibration ($\nu_{C\text{-}C}/\delta_{C\text{-}H}$) of ethylene glycol-derived species [49], while the band at 1432 cm^{-1} was attributable to the deformation vibration of NH$_3$ coordinated to the metal site. As a consequence, the intensity of the latter band was used as a descriptor of the amount of NH$_3$ adsorbed on the Co surface.
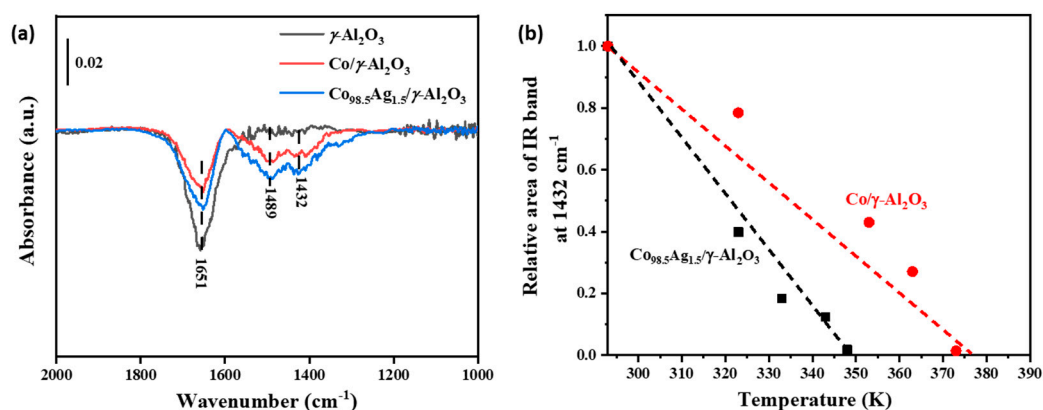
Figure 8. (**a**) Diffuse reflectance infrared Fourier transform spectra of NH$_3$-adsorbed Co/γ-Al$_2$O$_3$, Co$_{98.5}$Ag$_{1.5}$/γ-Al$_2$O$_3$, and γ-Al$_2$O$_3$ samples at 343 K (using the spectra collected at ambient temperature as the background); (**b**) the relative intensity of the adsorbed NH$_3$ species on metallic Co sites (1432 cm^{-1}) as a function of the desorption temperature for Co/γ-Al$_2$O$_3$ and Co$_{98.5}$Ag$_{1.5}$/γ-Al$_2$O$_3$.

As shown in Figure 8b, the desorption of NH$_3$ gradually occurred on both of Co/γ-Al$_2$O$_3$ and Co$_{98.5}$Ag$_{1.5}$/γ-Al$_2$O$_3$ as the temperature increased from 293 to 393 K (detailed spectra shown in Figure S12). It is noticeable that the bimetallic Co$_{98.5}$Ag$_{1.5}$/γ-Al$_2$O$_3$ catalyst completed the desorption at a temperature apparently lower than that for Co/γ-Al$_2$O$_3$ (348 vs. 373 K). This result indicated that the adsorption of NH$_3$ on Co$_{98.5}$Ag$_{1.5}$/γ-Al$_2$O$_3$ was weaker than on Co/γ-Al$_2$O$_3$, consistent with the above kinetic assessment. This spectroscopic evidence clearly unveiled the unique ability of the Ag dopant in destabilizing the NH$_3$ species bound to the Co surface, although the effect of Ag-doping on the electronic state of the Co sites was not observable from the deformation vibration bond of the adsorbed NH$_3$. More efforts are still required to understand the nature of the Ag-doping effects for ammonolysis of ethylene glycol on Co-based catalysts.

3. Experimental

3.1. Preparation of Supported Co Catalysts

Co/γ-Al_2O_3 catalysts (Co loading: 2, 5, 10, and 15 wt%) were prepared by the conventional incipient wetness impregnation method [34]. Using 5 wt% Co/γ-Al_2O_3 as an example, 0.617 g $Co(NO_3)_2 \cdot 6H_2O$ (AR, Sinopharm Chemical, Shanghai, China) was dissolved in 1.5 mL deionized water. This aqueous solution was then added dropwise to the γ-Al_2O_3 support (Sigma-Aldrich, Waltham, MA, USA, 154 $m^2 \cdot g^{-1}$) of 2.38 g, and the resultant powder was dried in an oven at 393 K overnight. Subsequently, the dried powder was treated in stagnant air at 673 K for 4 h (2 K min^{-1}) to decompose the $Co(NO_3)_2$ precursor to form Co_2O_3/γ-Al_2O_3, followed by a reduction process in flowing H_2 (40 mL min^{-1}, ≥99.999%, Linde Gases, Shanghai, China) at 773 K for 1 h (2 K min^{-1}) to obtain the Co/γ-Al_2O_3 catalysts. Bimetallic Co-M$/\gamma$-Al_2O_3 catalysts (M = Cu, Ag, Ru) with the Co loading fixed at 5 wt% were prepared through co-impregnation, in which $Cu(NO_3)_2 \cdot 3H_2O$ (AR, Sinopharm Chemical), $AgNO_3$ (AR, Sinopharm Chemical), and $RuCl_3 \cdot 3H_2O$ (98%, Energy Chemical, Shanghai, China) were chosen as the precursors of the second metal. The thermal treatments for the resultant bimetallic samples were identical to that in the preparation of the Co/γ-Al_2O_3 catalysts.

3.2. Catalyst Characterization

Powder X-ray diffraction (XRD) patterns of the Co-based catalysts were recorded in the 2θ range of 10–90° (scan speed 0.167°·s^{-1}) on a Panalytical X'Pert PRO diffractometer (Cu K_α radiation, λ = 0.15406 nm) at 40 kV and 30 mA. Transmission electron microscopy (TEM) images were collected on a Tecnai G2 F20 transmission electron microscope (FEI) operating at 200 kV. Before measurements, the samples were ultrasonically dispersed in ethanol solvent and then loaded onto carbon-coated Cu grids. The average size of metal particles was calculated on the basis of ca. 200 particles in different regions of the TEM images. Ex-situ X-ray photoelectron spectroscopy (XPS) spectra of the catalysts were recorded at 12 kV using a Thermo Scientific K-Alpha spectrometer equipped with a monochromatic Al K_α radiation source. The binding energy (BE) values were referred to the C 1s peak at 284.8 eV. The metal loading of the supported catalysts was determined by the inductively coupled plasma optical emission spectrometry (ICP, Thermo Fisher Scientific, ICAP7400).

The reducibility of the oxide form of the Co-based catalysts was assessed via H_2-temperature-programmed reduction (H_2-TPR) tests on a fully-automated chemisorption analyzer (DAS-7200, HUASI). Each sample (100 mg) was first treated in flowing N_2 (40 mL min^{-1}, >99.999%, Linde Gases) at 573 K for 1 h to remove physical adsorbed H_2O. After the temperature decreased to 313 K, the gas was switched to 5% H_2/Ar mixture (40 mL min^{-1}, Linde Gases), and the sample was heated to 1173 K at a ramp rate of 10 K min^{-1}. The H_2-TPR profiles were recorded and quantified using a thermal conductivity detector.

The dispersion of metallic Co for the Co-based catalysts was measured by the N_2O-chemisorption method [38,50] on the same chemisorption analyzer. Each pre-reduced catalyst (100 mg) was first exposed to a 5% N_2O/N_2 flow (60 mL min^{-1}, Linde Gases) at 323 K for 1 h to selectively oxidize the surface of the Co nanoparticles. The amount of chemically-adsorbed O atoms on the Co nanoparticles was determined from a subsequent H_2-TPR process using the protocol described above. The dispersion of Co was then calculated based on the hypothesis that metallic Co can be oxidized to Co^{3+} by N_2O under the chemisorption condition, and the average size of the Co nanoparticles ($<d>$, unit in nm) was estimated according to the following equation [51,52],

$$Dispersion = \frac{96}{\langle d \rangle} \times 100\% \tag{3}$$

which assumes a spherical geometry of the Co nanoparticles.

Diffuse reflectance infrared Fourier transform spectroscopy (DRIFTS) was employed for monitoring the desorption of NH_3 on Co/γ-Al_2O_3, $Co_{98.5}Ag_{1.5}/\gamma$-Al_2O_3, and γ-Al_2O_3

as a function of temperature, which were carried out using a Nicolet iS50 FT-IR spectrometer (Thermo Fisher Scientific, Waltham, MA, USA) equipped with a MCT/A detector (4 cm^{-1} resolution, 64 scans for each spectrum). The pre-adsorption of NH$_3$ for each sample was conducted in a stainless-steel autoclave under the real condition of ethylene glycol ammonolysis (453 K, 0.067 mol L^{-1} ethylene glycol in tetrahydrofuran, 0.6 MPa NH$_3$, 3.0 MPa H$_2$) for 0.5 h. The resultant powder was separated without further washing by any solvent and then dried in a vacuum oven at 303 K for 12 h. Background spectra were collected at ambient temperature after the IR cell was purged by a He flow. The cell was heat stepwise in flowing H$_2$ from 293 to 393 K (10 K per step, 5 K min^{-1} of the ramp rate), and the IR spectra of the samples were collected at each step after the temperature kept stable for 0.5 h.

3.3. Catalytic Ammonolysis of Ethylene Glycol

Ammonolysis of ethylene glycol was carried out in a 50 mL stainless-steel autoclave (HAC-1040, HUASI, Changsha, China). In a typical test, 0.124 g ethylene glycol (AR, Sinopharm Chemical) and 15 mL tetrahydrofuran solvent (AR, Sinopharm Chemical), together with 0.100 g Co-based catalyst (ground powder, <0.075 mm) pre-reduced at 773 K by H$_2$ as described in Section 3.1, were added into the autoclave. The reactor was then sealed and purged three times with pure NH$_3$ gas. After 0.6 MPa NH$_3$ and 3.0 MPa H$_2$ were added sequentially into the autoclave, the ammonolysis of ethylene glycol was conducted at 453 K under stirring (800 rpm) for 2–4 h. It was confirmed that the possibility of mass transport limitations was excluded at the conditions of our kinetic measurements based on the tests of the stirring speed and the catalyst particle size (Figures S13 and S14). After the reaction, the liquid phase and the catalyst were separated by centrifugation. The concentrations of ethylene glycol and reaction products were quantitively analyzed off-line by gas chromatography (GC7820, Shandong Huifen) with an OV-1701 capillary column connected to a flame ionization detector, and isopropanolamine (AR, Sinopharm Chemical) was selected as the internal standard. These products were identified using known standards and speciation by mass spectrometry after chromatographic separations (Agilent 7890B-5977BGC/MSD). The carbon balance was accurate to within 6% for each catalytic test. The conversion of ethylene glycol (C_{EG}) and the selectivity of product i (S_i) were calculated as reported elsewhere [34]:

$$C_{EG}\ (\%) = \frac{n_{EG}^0 - n_{EG}}{n_{EG}^0} \tag{4}$$

$$S_i\ (\%) = \frac{\alpha_i \times n_i}{2 \times \left(n_{EG}^0 - n_{EG}\right)} \tag{5}$$

Here, n_{EG}^0 and n_{EG} refer to the initial and final molar amounts of ethylene glycerol in the reactor, respectively, n_i is the molar amount of product i formed after the reaction, and α_i is the carbon number of product i. Rates of ethylene glycol conversion were calculated based on both of the surface Co atoms (i.e., turnover frequency) and the total Co amount. The regressed fitting of these rates with the proposed kinetic equations was conducted using the Bayesian estimation method, as implemented in the Athena Visual Studio software package.

4. Conclusions

For the liquid-phase ammonolysis of ethylene glycol on Co/γ-Al$_2$O$_3$ catalysts, a moderate size of the Co nanoparticles (~4 nm) is a requisite for obtaining both of a high amination rate and a high chemoselectivity to ethanolamine. Smaller Co nanoparticles (~2 nm) are not only intrinsically less active in the ammonolysis of ethylene glycol but also exhibit a higher selectivity to glycolaldehyde due to the lack of enough ability in catalyzing the condensation between glycolaldehyde and NH$_3$. The activity of the Co/γ-Al$_2$O$_3$ catalysts can be further improved by adding a moderate amount of Cu, Ag, or

Ru, while the high chemoselectivity to ethanolamine is only maintained in the case of Ag-doping. Combined kinetic and infrared spectroscopic assessments reveal that the dehydrogenation of ethylene glycol to glycolaldehyde is the rate-limiting step for ethylene glycol ammonolysis on the Co-based catalysts, the surface of which is highly covered by NH_3 species at the reaction condition. The introduction of Ag dopant weakens the adsorption of NH_3 on the Co surface and renders more Co sites available for catalyzing ethylene glycol dehydrogenation, which accounts for the promoting effect of Ag-doping on the ammonolysis activity of the $Co/\gamma-Al_2O_3$ catalysts.

Supplementary Materials: The following are available online at https://www.mdpi.com/article/10.3390/catal11060736/s1, Figure S1: Powder XRD patterns for Co/γ-Al2O3 samples (Co 2 wt%-15 wt%) and the γ-Al2O3 support with metallic Co (JCPDS 15-0806) as reference, Figure S2: H2-TPR profiles for (a) the oxide persursors of the Co/γ-Al2O3 catalysts (Co 2 wt%–15 wt%) and (b) the Co/γ-Al2O3 catalysts after treated in flowing 5% N2O/N2 at 323 K for 1 h, Figure S3: TEM image for (a) 5 wt% Co/γ-Al2O3 with (b) the corresponding statistic size distribution of the Co nanoparticles, Figure S4: TEM image for (a) Co98.5Ag1.5/γ-Al2O3 with (b) the corresponding statistic size disturibution of the Co nanoparticles, Figure S5: Detailed product disturibution of the ammonolysis of ethylene glycol on Co98.5M1.5/γ-Al2O3 (M = Cu, Ag, and Ru; 5 wt% Co) catalysts at ~20% conversion (453 K, 0.6 MPa NH3, 3.0 MPa H2, 0.067 mol/L ethylene glycol in tetrahydrofuran solution, 2 h), Figure S6: Activity comparison among 5 wt% Co/γ-Al2O3, 5 wt% Co98.5Ag1.5/γ-Al2O3, and 5 wt% Ag/γ-Al2O3 in catalytic ammonolysis of ethylene glycol (453 K, 0.6 MPa NH3, 3.0 MPa H2, 0.067 mol/L ethylene glycol in tetrahydrofuran solution, 2 h), Figure S7: (a) Co 2p and (b) Ag 3d XPS spectra for the Co98.5Ag1.5/γ-Al2O3 and Co95Ag5/γ-Al2O3 catalysts and (c) the corresponding Ag/(Co+Ag) surface ratios determined from these spectra, Figure S8: Selectivities of ethylene glycol concentration on (a) Co/γ-Al2O3 and (b) Co98.5Ag1.5/γ-Al2O3 catalysts (Co 5 wt%) as a function of ethylene glycol concentration (453 K, 0.6 MPa NH3, 3.0 MPa H2, 2 h, ~20% ethylene glycol conversion obtained by varying the catalyst amount or reaction time), Figure S9: Selectivities of ethylene glycol concentration on (a) Co/γ-Al2O3 and (b) Co98.5Ag1.5/γ-Al2O3 catalysts (Co 5 wt%) as a function of NH3 pressure (453 K, 3.0 MPa H2, 0.067 mol/L ethylene glycol in tetrahydrofuran solution, 2 h, ~20% ethylene glycol conversion obtained by varying the catalyst amount or reaction time), Figure S10: Selectivities of ethylene glycol concentration on (a) Co/γ-Al2O3 and (b) Co98.5Ag1.5/γ-Al2O3 catalysts (Co 5 wt%) as a function of H2 pressure (453 K, 0.6 MPa NH3, 0.067 mol/L ethylene glycol in tetrahydrofuran solution, 2 h, ~20% ethylene glycol conversion obtained by varying the catalyst amount or reaction time), Figure S11: A parity plot for the measured and predicted rates of ethylene glycol amination (Equation (2)) on the Co/γ-Al2O3 and Co98.5Ag1.5/γ-Al2O3 catalysts, Figure S12: Infrared spectra of NH3 desorption as a function of temperature for (a) Co/γ-Al2O3 and (b) Co98.5Ag1.5/γ-Al2O3 (using the respective spectra collected at ambient temperature as the background), Figure S13: Effect of stirring speed on the rate of ethylene glycol ammonolysis over 5 wt% Co/γ-Al2O3 (453 K, 0.6 MPa NH3, 3.0 MPa H2, 0.067 mol/L ethylene glycol in tetrahydrofuran solution, 2 h), Figure S14: Effect of particle size on the rate of ethylene glycol ammonolysis over 5 wt% Co/γ-Al2O3 (453 K, 0.6 MPa NH3, 3.0 MPa H2, 0.067 mol/L ethylene glycol in tetrahydrofuran solution, 2 h).

Author Contributions: S.W. conceived the idea for the project. X.L., G.G. and Y.H. conducted the catalyst synthesis and structural characterization. X.L. and H.W. performed the catalytic tests. X.L. drafted the manuscript under the guidance of S.W. and Z.Z. All authors discussed and commented on the manuscript. All authors have read and agreed to the published version of the manuscript.

Conflicts of Interest: The authors declare that they have no competing interest.

References

1. Yue, H.; Zhao, Y.; Ma, X.; Gong, J. Ethylene glycol: Properties, synthesis, and applications. *Chem. Soc. Rev.* **2012**, *41*, 4218–4244. [CrossRef] [PubMed]
2. Marchesan, A.N.; Oncken, M.P.; Filho, R.M.; Maciel, M.R.W. A roadmap for renewable C2–C3 glycols production: A process engineering approach. *Green Chem.* **2019**, *21*, 5168–5194. [CrossRef]
3. Wang, Z.-Q.; Sun, J.; Xu, Z.-N.; Guo, G.-C. CO direct esterification to dimethyl oxalate and dimethyl carbonate: The key functional motifs for catalytic selectivity. *Nanoscale* **2020**, *12*, 20131–20140. [CrossRef]
4. Faveere, W.H.; van Praet, S.; Vermeeren, B.; Dumoleijn, K.N.R.; Moonen, K.; Taarning, E.; Sels, B.F. Toward replacing ethylene oxide in a sustainable world: Glycolaldehyde as bio-based C2 platform molecule. *Angew. Chem. Int. Ed.* **2020**, *59*, 2–22.
5. Liang, G.; Wang, A.; Li, L.; Xu, G.; Yan, N.; Zhang, T. Production of Primary Amines by Reductive Amination of Biomass-Derived Aldehydes/Ketones. *Angew. Chem. Int. Ed.* **2017**, *56*, 3050–3054. [CrossRef]
6. Fischer, A.; Mallat, T.; Baiker, A. Amination of diols and polyols to acyclic amines. *Catal. Today* **1997**, *37*, 167–189. [CrossRef]
7. Pelckmans, M.; Renders, T.; Van de Vyver, S.; Sels, B.F. Bio-based amines through sustainable heterogeneous catalysis. *Green Chem.* **2017**, *19*, 5303–5331. [CrossRef]
8. Wang, X.; Wang, H.; Shi, F. 7-Alcohol Amination for N-Alkyl Amine Synthesis with Heterogeneous Catalysts. *Process. Chem.* **2020**, *32*, 162–178.
9. Wu, Y.; Yuan, H.; Shi, F. Sustainable Catalytic Amination of Diols: From Cycloamination to Monoaminatio. *ACS Sustain. Chem Eng.* **2018**, *6*, 1061–1067. [CrossRef]
10. Ho, C.R.; Defalque, V.; Zheng, S.; Bell, A.T. Propanol Amination over Supported Nickel Catalysts: Reaction Mechanism and Role of the Support. *ACS Catalysis* **2019**, *9*, 2931–2939. [CrossRef]
11. Shimizu, K.-I.; Kon, K.; Onodera, W.; Yamazaki, H.; Kondo, J. Heterogeneous Ni Catalyst for Direct Synthesis of Primary Amines from Alcohols and Ammonia. *ACS Catalysis* **2012**, *3*, 112–117. [CrossRef]
12. Bassili, V.A.; Baiker, A. Catalytic amination of 1-methoxy-2-propanol over silica supported nickel: Study of the influence of the reaction parameters. *Appl. Catal.* **1990**, *65*, 293–308. [CrossRef]
13. Pera-Titus, M.; Shi, F. Catalytic Amination of Biomass-Based Alcohols. *ChemSusChem* **2014**, *7*, 720–722. [CrossRef] [PubMed]
14. Bähn, S.; Imm, S.; Neubert, L.; Zhang, M.; Neumann, H.; Beller, M. The Catalytic Amination of Alcohols. *ChemCatChem* **2011**, *3*, 1853–1864. [CrossRef]
15. Guillena, G.; Ramon, D.J.; Yus, M. Hydrogen Autotransfer in the N-Alkylation of Amines and Related Compounds using Al-cohols and Amines as Electrophiles. *Chem. Rev.* **2010**, *110*, 1611–1641. [CrossRef] [PubMed]
16. Hamid, M.H.S.A.; Slatford, P.A.; Williams, J.M.J. Borrowing Hydrogen in the Activation of Alcohols. *Adv. Synth. Catal.* **2007**, *349*, 1555–1575. [CrossRef]
17. Jagadeesh, R.V.; Stemmler, T.; Surkus, A.E.; Bauer, M.; Pohl, M.M.; Radnik, J.; Junge, K.; Junge, H.; Bruckner, A.; Beller, M. Co-balt-based nanocatalysts for green oxidation and hydrogenation processes. *Nat. Protoc.* **2015**, *10*, 916–926. [CrossRef]
18. Jagadeesh, R.V.; Murugesan, K.; Alshammari, A.S.; Neumann, H.; Pohl, M.-M.; Radnik, J.; Beller, M. MOF-derived cobalt na-noparticles catalyze a general synthesis of amines. *Science* **2017**, *358*, 326–332. [CrossRef]
19. Murugesan, K.; Chandrashekhar, V.; Senthamarai, T.; Jagadeesh, R.V.; Beller, M. Reductive amination using cobalt-based nanoparticles for synthesis of amines. *Nat. Protoc.* **2020**, *15*, 1313–1337. [CrossRef]
20. Hahn, G.; Kunnas, P.; De Jonge, N.; Kempe, R. General synthesis of primary amines via reductive amination employing a reusable nickel catalyst. *Nat. Catal.* **2018**, *2*, 71–77. [CrossRef]
21. Murugesan, K.; Beller, M.; Jagadeesh, R.V. Reusable Nickel Nanoparticles-Catalyzed Reductive Amination for Selective Synthesis of Primary Amines. *Angew. Chem. Int. Ed.* **2019**, *58*, 5064–5068. [CrossRef] [PubMed]
22. Sun, M.; Du, X.; Wang, H.; Wu, Z.; Li, Y.; Chen, L. Reductive Amination of Triacetoneamine with n-Butylamine Over Cu–Cr–La/γ-Al2O3. *Catal. Lett.* **2011**, *141*, 1703–1708. [CrossRef]
23. Liang, G.; Zhou, Y.; Zhao, J.; Khodakov, A.Y.; Ordomsky, V.V. Structure-Sensitive and Insensitive Reactions in Alcohol Ami-nation over Nonsupported Ru Nanoparticles. *ACS Catalysis* **2018**, *8*, 11226–11234. [CrossRef]
24. Xie, C.; Song, J.; Hua, M.; Hu, Y.; Huang, X.; Wu, H.; Yang, G.; Han, B. Ambient-Temperature Synthesis of Primary Amines via Reductive Amination of Carbonyl Compounds. *ACS Catalysis* **2020**, *10*, 7763–7772. [CrossRef]
25. Furukawa, S.; Suzuki, R.; Komatsu, T. Selective Activation of Alcohols in the Presence of Reactive Amines over Intermetallic PdZn: Efficient Catalysis for Alcohol-Based N-Alkylation of Various Amines. *ACS Catalysis* **2016**, *6*, 5946–5953. [CrossRef]
26. Tong, T.; Guo, W.; Liu, X.; Guo, Y.; Pao, C.-W.; Chen, J.-L.; Hu, Y.; Wang, Y. Dual functions of CoOx decoration in PtCo/CeO2 catalysts for the hydrogen-borrowing amination of alcohols to primary amines. *J. Catal.* **2019**, *378*, 392–401. [CrossRef]
27. Wu, Y.; Gui, W.; Liu, X.; Zhang, L.; Wang, S.; Wang, Z.; Zhang, C. Promotional Effect of Cu for Catalytic Amination of Diethylene Glycol with Tertiarybutylamine over Ni–Cu/Al2O3 Catalysts. *Catal. Lett.* **2020**, *150*, 2427–2436. [CrossRef]
28. Ibáñez, J.; Araque, M.; Paul, S.; Pera-Titus, M. Direct amination of 1-octanol with NH3 over Ag-Co/Al2O3: Promoting effect of the H2 pressure on the reaction rate. *Chem. Eng. J.* **2019**, *358*, 1620–1630. [CrossRef]
29. Wang, T.; Ibañez, J.; Wang, K.; Fang, L.; Sabbe, M.; Michel, C.; Paul, S.; Pera-Titus, M.; Sautet, P. Rational design of selective metal catalysts for alcohol amination with ammonia. *Nat. Catal.* **2019**, *2*, 773–779. [CrossRef]
30. Niu, F.; Bahri, M.; Ersen, O.; Yan, Z.; Kusema, B.T.; Khodakov, A.Y.; Ordomsky, V.V. A multifaceted role of a mobile bismuth promoter in alcohol amination over cobalt catalysts. *Green Chem.* **2020**, *22*, 4270–4278. [CrossRef]

31. Ma, L.; Yan, L.; Lu, A.-H.; Ding, Y. Effects of Ni particle size on amination of monoethanolamine over Ni-Re/SiO2 catalysts. *Chin. J. Catal.* **2019**, *40*, 567–579. [CrossRef]

32. Zhang, C.; Li, S.; Wu, C.; Li, X.; Yan, X. Preparation and Characterization of Pt@Au/Al2O3 Core-Shell Nanoparticles for Toluene Oxidation Reaction. *Acta Physico-Chimica Sinica* **2020**, *36*, 1907057. [CrossRef]

33. Niu, F.; Xie, S.; Yan, Z.; Kusema, B.T.; Ordomsky, V.V.; Khodakov, A.Y. Alcohol amination over titania-supported ruthenium nanoparticles. *Catal. Sci. Technol.* **2020**, *10*, 4396–4404. [CrossRef]

34. Ibáñez, J.; Kusema, B.T.; Paul, S.; Pera-Titus, M.; Abad, J.I. Ru and Ag promoted Co/Al2O3 catalysts for the gas-phase amination of aliphatic alcohols with ammonia. *Catal. Sci. Technol.* **2018**, *8*, 5858–5874. [CrossRef]

35. Jongsomjit, B.; Panpranot, J.; Goodwin, J.G. Co-Support Compound Formation in Alumina-Supported Cobalt Catalysts. *J. Catal.* **2001**, *204*, 98–109. [CrossRef]

36. Najafabadi, A.T.; Khodadadi, A.A.; Parnian, M.J.; Mortazavi, Y. Atomic layer deposited Co/γ-Al2O3 catalyst with enhanced cobalt dispersion and Fischer–Tropsch synthesis activity and selectivity. *Appl. Catal. A Gen.* **2016**, *511*, 31–46. [CrossRef]

37. Van der Grift, C.J.G.; Wielers, A.F.H.; Joghi, B.P.J.; van Beijnum, J.; de Boer, M.; Versluijs-Helder, M.; Geus, J.W. Effect of the reduction treatment on the structure and reactivity of silica-supported copper particles. *J. Catal.* **1991**, *131*, 178–189. [CrossRef]

38. Huang, Z.; Chen, J.; Jia, Y.; Liu, H.; Xia, C.; Liu, H. Selective hydrogenolysis of xylitol to ethylene glycol and propylene glycol over copper catalysts. *Appl. Catal. B Environ.* **2014**, *147*, 377–386. [CrossRef]

39. Wang, Y.; Furukawa, S.; Fu, X.; Yan, N. Organonitrogen Chemicals from Oxygen-Containing Feedstock over Heterogeneous Catalysts. *ACS Catalysis* **2020**, *10*, 311–335. [CrossRef]

40. Baiker, A.; Caprez, W.; Holstein, W.L. Catalytic amination of aliphatic alcohols in the gas and liquid phases: Kinetics and reaction pathway. *Ind. Eng. Chem. Prod. Res. Dev.* **1983**, *22*, 217–225. [CrossRef]

41. Runeberg, J.; Baiker, A.; Kijenski, J. Copper catalyzed amination of ethylene glycol. *Appl. Catal.* **1985**, *17*, 309–319. [CrossRef]

42. Dumon, A.S.; Wang, T.; Ibanez, J.; Tomer, A.; Yan, Z.; Wischert, R.; Sautet, P.; Pera-Titus, M.; Michel, C. Direct n-octanol amination by ammonia on supported Ni and Pd catalysts: Activity is enhanced by "spectator" ammonia adsorbates. *Catal. Sci. Technol.* **2018**, *8*, 611–621. [CrossRef]

43. Yue, C.-J.; Di, K.; Gu, L.-P.; Zhang, Z.-W.; Ding, L.-L. Selective amination of 1,2-propanediol over Co/La3O4 catalyst prepared by liquid-phase reduction. *Mol. Catal.* **2019**, *477*, 110539. [CrossRef]

44. Fu, X.-P.; Han, P.; Wang, Y.-Z.; Wang, S.; Yan, N. Insight into the roles of ammonia during direct alcohol amination over supported Ru catalysts. *J. Catal.* **2021**, *399*, 121–131. [CrossRef]

45. Mamontov, G.V.; Grabchenko, M.V.; Sobolev, V.I.; Zaikovskii, V.I.; Vodyankina, O.V. Ethanol dehydrogenation over Ag-CeO2/SiO2 catalyst: Role of Ag-CeO2 interface. *Appl. Catal. A* **2016**, *528*, 161–167. [CrossRef]

46. Liu, H.; Tan, H.-R.; Tok, E.S.; Jaenicke, S.; Chuah, G.-K. Dehydrogenation of Alcohols over Alumina-Supported Silver Catalysts: The Role of Oxygen in Hydrogen Formation. *ChemCatChem* **2016**, *8*, 968–975. [CrossRef]

47. Hu, H.; Cai, S.; Li, H.; Huang, L.; Shi, L.; Zhang, D. In Situ DRIFTs Investigation of the Low-Temperature Reaction Mechanism over Mn-Doped Co3O4 for the Selective Catalytic Reduction of NOx with NH3. *J. Phys. Chem. C* **2015**, *119*, 22924–22933. [CrossRef]

48. Meng, D.; Zhan, W.; Guo, Y.; Guo, Y.; Wang, L.; Lu, G. A Highly Effective Catalyst of Sm-MnOx for the NH3-SCR of NOx at Low Temperature: Promotional Role of Sm and Its Catalytic Performance. *ACS Catalysis* **2015**, *5*, 5973–5983. [CrossRef]

49. Kim, K.; Park, A.H.K.; Kim, N.H. Silver-Particle-Based Surface-Enhanced Raman Scattering Spectroscopy for Biomolecular Sensing and Recognition. *Langmuir* **2006**, *22*, 3421–3427. [CrossRef]

50. Tada, S.; Yokoyama, M.; Kikuchi, R.; Haneda, T.; Kameyama, H. N2O Pulse Titration of Ni/α-Al2O3 Catalysts: A New Technique Applicable to Nickel Surface-Area Determination of Nickel-Based Catalysts. *J. Phys. Chem. C* **2013**, *117*, 14652–14658. [CrossRef]

51. Jones, R.D.; Bartholomew, C.H. Improved flow technique for measurement of hydrogen chemisorption on metal catalysts. *Appl. Catal.* **1988**, *39*, 77–88. [CrossRef]

52. Martínez, A.; López, C.; Márquez, F.; Díaz, I. Fischer–Tropsch synthesis of hydrocarbons over mesoporous Co/SBA-15 catalysts: The influence of metal loading, cobalt precursor, and promoters. *J. Catal.* **2003**, *220*, 486–499. [CrossRef]